Macromolecules

ARTICLE

pubs.acs.org/Macromolecules

Induction Curing of Thiol−Acrylate and Thiol−Ene Composite Systems

Sheng Ye,[†] Neil B. Cramer,[†] Blake E. Stevens,[†] Robert L. Sani,[†] and Christopher N. Bowman*[,†,‡]

[†]Department of Chemical & Biological Engineering, University of Colorado, UCB 424, Boulder, Colorado 80309, United States

[‡]Department of Restorative Dentistry, University of Colorado School of Dentistry, Aurora, Colorado 80045, United States

ABSTRACT: Induction curing is demonstrated as a novel type of *in situ* radiation curing that maintains most of the advantages of photocuring while eliminating the restriction of light accessibility. Induction curing is utilized to polymerize opaque composites comprised of thiol−acrylate and thiol−ene resins, nanoscale magnetic particles, and carbon nanotubes. Nanoscale magnetic particles are dispersed in the resin, and upon exposure to the magnetic field, these particles lead to induction heating that rapidly initiates the polymerization. Heat transfer profiles and reaction kinetics of the samples are modeled during the reactions with varying induction heater power, species concentration, species type, and sample thickness, and the model is compared with the experimental results. Thiol−ene polymerizations achieved full conversion between 1.5 min and 1 h, depending on the field intensity and the composition, with the maximum reaction temperature decreasing from 146 to 87 °C when the induction heater power was decreased from 8 to 3 kW. The polymerization reactions of the thiol−acrylate system were demonstrated to achieve full conversion between 0.6 and 30 min with maximum temperatures from 139 to 86 °C. The experimental behavior was characterized and the temperature profile modeled for the thiol−acrylate composite comprised of sub-100 nm nickel particles and induction heater power in the range of 32−20 kW. A 9 °C average deviation was observed between the modeling and experimental results for the maximum temperature rise. The model also was utilized to predict reaction temperatures and kinetics for systems with varying thermal initiator concentration, initiator half-life, monomer molecular weight, and temperature gradients in samples with varying thickness, thereby demonstrating that induction curing represents a designable and tunable polymerization method. Finally, induction curing was utilized to cure thiol−acrylate systems containing carbon nanotubes where 1 wt % carbon nanotubes resulted in systems where the storage modulus increased from 17.6 ± 0.2 to 21.6 ± 0.1 MPa and an electrical conductivity that increased from $<10^{-7}$ to 0.33 ± 0.5 S/m.

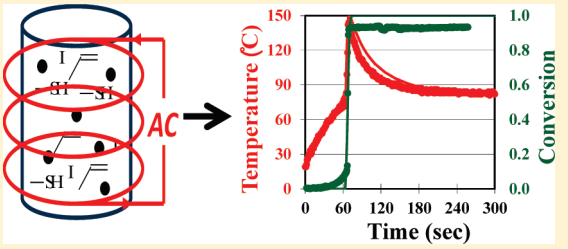

INTRODUCTION

The vast majority of radical polymerizations are initiated via thermal heating. The heat source is provided externally to the target, which in some cases can result in temperature gradients, reaction rate gradients, and nonuniform material properties. Also, traditional heating techniques are limited to applications that do not involve temperature-sensitive substrates. Radiation curing is an alternative radical polymerization methodology that represents a highly desirable method for producing cross-linked polymer networks with advantages that include spatiotemporal control of the reaction, solvent-free formulations, ambient curing, and high energy efficiency.[1,2] X-ray and γ-ray initiation are two forms of radiation curing that have been studied but have only seen limited application because of the hazards associated with these wavelengths to the human body and the subsequent requirements for shielding. Far more commonly, radiation curing utilizes ultraviolet or visible light with widespread applications that include lithography, dental materials, printing inks, and clear coatings, to name a few.[3] However, in some applications, such as highly filled composite systems, pigmented systems, or systems that are inaccessible to light, photopolymerizations are limited by optical accessibility. In this work we describe a novel radio-frequency curing technique, induction curing, that combines aspects of both radiation and thermal curing. Induction curing maintains most of the advantages of photocuring such as rapid, efficient cure with temporal control while being an environmentally friendly technique that cures without the need for solvents. Moreover, induction curing eliminates the restriction of light accessibility that is required in traditional photocuring. Thus, induction curing is demonstrated to be a tunable and promising *in situ* polymerization method.

Induction heating is the process whereby a ferromagnetic material is exposed to an alternating magnetic field. Heat is generated by magnetization/demagnetization reversal losses (core loss), which usually consists of eddy current loss, hysteresis loss, and excess eddy current loss (sometimes referred to as anomalous or dynamic losses). Eddy current loss is a direct consequence of joule heating from electric currents induced in the material by the changing magnetization; hysteresis loss is caused by the continuous distortion of the ferromagnetic

Received: January 14, 2011
Revised: May 21, 2011
Published: June 01, 2011

crystalline structure (i.e., magnetic domain walls), and the excess eddy current loss has contributions from the magnetic domain-wall dynamics with size scales on the order of the microstructural features.[4−6] When the ferromagnetic particles are micro- or nanoscale, eddy current and excess eddy current losses dramatically diminish as the spatial dimensions of the conductor become very small; therefore, hysteresis loss is regarded as the sole heat generation mechanism. Thus, the induction heating technique can also be considered hysteresis heating when using microscale ferromagnetic particles.[7]

Hysteresis losses of different ferromagnetic materials are limited by their Curie temperature. The Curie temperature is a critical temperature, above which magnetic domains are randomly aligned and no hysteresis loss is generated.[5] Induction heating technology, as a simple way to increase temperature, has been widely utilized for decades in the metal industry for melting, brazing, forging, and annealing due to the advantages of rapid heating rate (materials achieve high temperatures within seconds), controlled local heating, no radiant heating to the environment, and high efficiency compared with conventional external heating methods.[8] In recent years, induction heating has been employed by embedding ferromagnetic particles in a thermoplastic matrix to achieve induction melting, welding,[9] coating,[10] shape memory polymers,[11,12] or adhesion of polymeric materials.[13,14] Suwanwatana and co-workers also developed a heat transfer model relating different nickel particle size, loading, magnetic field, and frequency to the temperature change in a cured polymer.[7,14] These studies utilized induction heating as a heat source to heat polymers.

Induction heating has not previously been utilized to induce an *in situ* radical polymerization of thiol-containing monomer formulations, and there has not been a model developed for an *in situ* induction polymerization which combines both induction heating process and reaction kinetics. For the induction heating polymerizations described herein, micro-ferromagnetic particles are dispersed in a reactive monomer system that also contains thermally sensitive radical initiators. Upon exposure to an alternating magnetic field, the heat generated by the particles heats the system and triggers cleavage of the thermal initiators, initiating the desired radical polymerization. Since the magnetic particles are the only component responding to the magnetic field, the reaction kinetics are not affected by the field itself aside from the temperature increase. By using this method, highly filled composite systems are radiation cured without the limitations of optical accessibility or the hazards associated with X-rays and γ-rays. Also, as compared to external heating techniques (i.e., oven heating), induction heating is much more rapid and efficient and essentially applies targeted heat to the ferromagnetic particles suspended in the resin while leaving any associated substrates only indirectly affected. Thus, induction heating polymerization has the potential for applications in coatings or adhesion to thermally sensitive materials.

In this work, thiol−ene and thiol−acrylate polymerizations have been chosen as model systems. Thiol−ene systems are an emerging area in photopolymerizations as they exhibit several unique, and often advantageous, properties such as delayed gelation, reduced oxygen inhibition, and low shrinkage stress.[1,15−17] These properties are a result of the unique free radical step-growth reaction mechanism. The step-growth mechanism involves a thiyl radical, which adds across an ene functional group to form a carbon-centered radical. The thiyl radical is subsequently regenerated by chain transfer of the carbon-centered radical to another thiol functional group.[18] Thiol−acrylate systems undergo a radical step-growth polymerization between thiols and acrylates and homopolymerization of acrylates, a process which maintain the advantages of thiol−ene systems while providing the ability to achieve higher glass transition temperatures.[18] Nickel and cobalt particles exhibit relatively good stability with thiol−ene and thiol−acrylate systems, are abundant in a variety of sizes, and are also inexpensive and are therefore good candidates as model particles for the induction heating process. Carbon nanotubes (CNTs) were chosen as a filler material based on their high aspect ratio, resulting in highly desirable modulus and conductivity properties.[19] Also, a heat transfer model of *in situ* induction polymerization was developed and confirmed by experimental data. The model also was utilized to predict reaction temperatures and kinetics for systems with varying thermal initiator concentration, initiator half-life, monomer molecular weight, and temperature gradients in samples with varying thickness.

EXPERIMENTAL SECTION

Trimethylolpropane tris(3-mercaptopropionate) (TMPTMP), allyl pentaerythritol (APE), and 2,2′-azobis(isobutyronitrile) (AIBN) were all purchased from Sigma-Aldrich Co. (Milwaukee, WI). Poly(ethylene glycol)200 diacrylate (PEGDA) was purchased from Sartomer Co. (Exton, PA). Pentaerythritol tetra(3-mercaptopropionate) (PETMP) was donated by Evans Chemetics; nanoscale (<100 nm) and microscale (3 μm) nickel particles and microscale (2 μm) cobalt particles were purchased from Sigma-Aldrich Co. (Milwaukee, WI). Multiwall hydroxyl functionalized carbon nanotubes (CNT-OH) were purchased from Nanostructured and Amorphous Materials Inc. with a 60−80 nm diameter range, 10−20 μm length range, and 95% purity. Conductive liquid silver paint was purchased form Jed Pella Inc. (Redding, CA). All materials were used without further purification.

Stoichiometric thiol to ene functional group ratios were used in the PETMP−APE resins, and 3:7 thiol to acrylate functional group ratios were used in the PETMP−PEGDA resins to minimize the amount of unreacted thiol monomers.[18] TMPTMP, PEGDA, magnetic particles, and CNT-OH were mixed for 5 min by an ultrasonic cell crusher (SYJ-650, Sharpertek Corp., Auburn Hills, MI) operating at 24 kHz. AIBN was added to the solution after sonication to prevent polymerization during mixing. The solution was then poured into a 20 × 5 × 0.8 mm cell, which was horizontally inserted into a solenoid coil where a vertical magnetic field was generated by an induction heater (7.5-135, Taylor-Winfield Corp., Brookfield, OH) with variable power settings.

Fourier transform infrared (FTIR) spectroscopy (Magna 750, series II, Nicolet Instrument Corp., Madison, WI) was utilized to monitor the functional group conversion. The near-IR light beam was aligned perpendicular to the sample with fiber-optic cables enabling real-time kinetic characterization. Conversion was monitored by observing the C═C vibration at 6020 cm^{-1}. An infrared pyrometer (Omega OS550) was arranged vertically to the sample to measure the temperature in real time during polymerization.

Dynamic mechanical analysis (DMA) was performed with a DMA Q800 dynamic mechanical analyzer (TA Instruments). The samples were rectangular films with dimensions of 20 × 5 × 0.8 mm. Multi-frequency strain mode was used to measure moduli as a function of temperature by applying a sinusoidal stress of frequency 1 Hz over a temperature range of −40 to 100 °C and a temperature ramping rate of 3 °C/min.

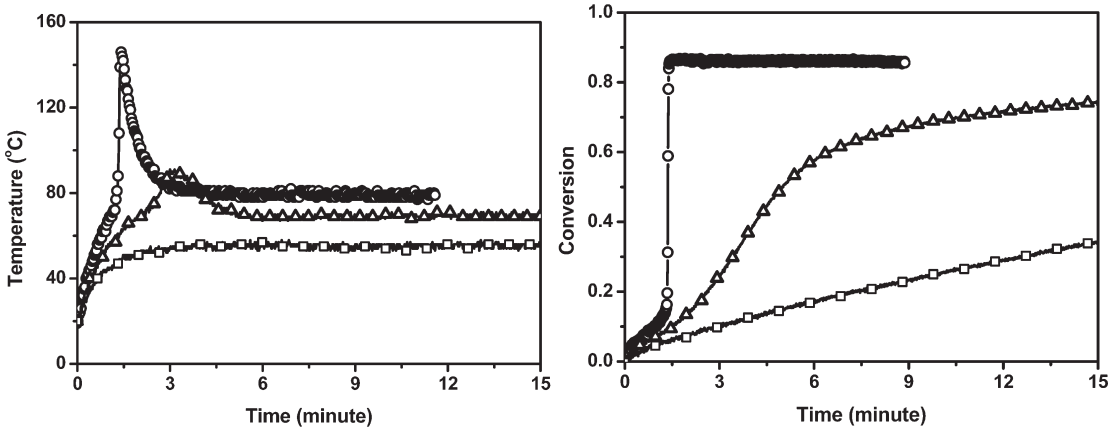

Figure 1. (a) Surface temperature versus time and (b) conversion versus time for PETMP−APE initiated by 1 wt % AIBN and 3 wt % Ni particles (3 μm) cured at induction heater powers of 8 (○), 6 (△), and 3 kW (□).

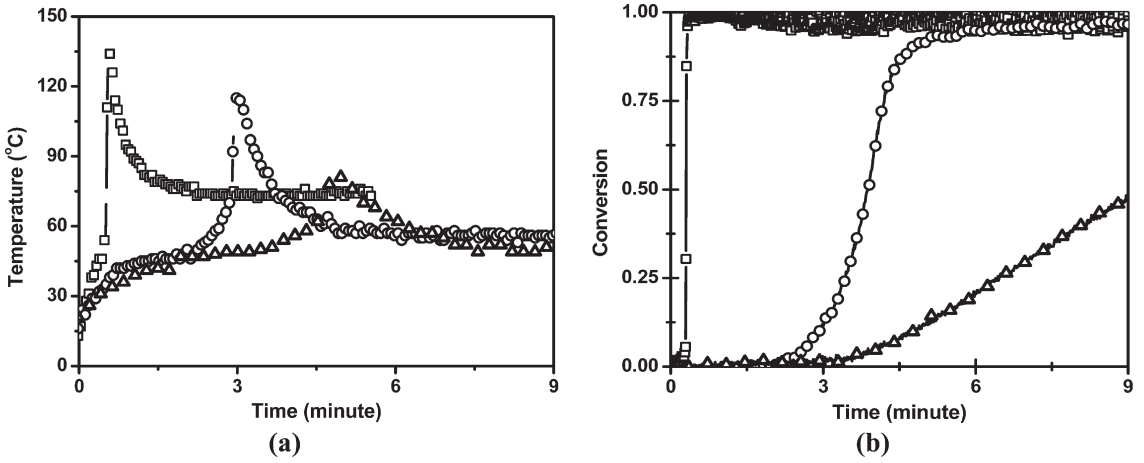

Figure 2. (a) Surface temperature versus time and (b) conversion versus time for PETMP−PEGDA initiated by 1 wt % AIBN and 1 wt % particles cured at 20 kW. Samples contain 2 μm cobalt (□), <100 nm nickel (○), and 3 μm nickel (△) particles.

Electrical conductivity of the composite material was calculated from the reciprocal of the resistivity measured by a Hewlett-Packard multimeter 34401 A (HP, Santa Clara, CA). The samples were coated with conductive silver paint to improve the contact between the probe and the polymer.

Scanning electron microscopy (SEM) (JSM-6480LV) with a low vacuum mode was utilized to observe the microstructure of the composite material by 5 kV. The samples were fractured under nitrogen and sputter-coated with gold.

■ RESULTS AND DISCUSSION

1. Kinetics of Thiol−Ene and Thiol−Acrylate Systems Cured by Induction Heating. To demonstrate the feasibility of induction curing of thiol−ene and thiol−acrylate systems, double-bond conversion and surface temperature versus time are shown in Figure 1 for a PETMP−APE system and in Figure 2 for a PETMP−PEGDA system. The reaction kinetics are strongly influenced by both induction heater power and the characteristics of the magnetic particles. In Figure 1, the PETMP−APE system achieves a final double bound conversion of 86% in 1.5 min at 8 kW, 84% in 1 h at 6 kW, and only 70% at 3 kW after 1 h. Higher induction heater power generates stronger magnetic fields, resulting in faster temperature ramping and reaction kinetics. The surface temperature profiles of the systems reacted at 8 and 6 kW show a relatively slow temperature increase resultant from induction heating of the nickel particles, followed by a rapid increase in temperature caused by the exothermic nature of the thiol−ene polymerization. The polymerization reaction begins to occur rapidly around 70 °C, which is the temperature where the cleavage rate of AIBN increases dramatically. The system reacted at 8 kW reaches a maximum temperature of 146 °C, whereas the system reacted at 6 kW reaches only 87 °C because of the slower reaction. There is no obvious reaction peak in the temperature profile of the system reacted at 3 kW because the temperature, limited by heat transfer to the environment, reaches only 56 °C, which does not result in sufficiently rapid cleavage of AIBN to initiate a viable polymerization. These results demonstrate that the reaction rate and the maximum temperature are controlled by adjusting the induction heater power. Figure 2 shows the double-bond conversion and surface temperature versus time of the PETMP−PEGDA system polymerized with different particle types and sizes. The system containing cobalt particles heats the most rapidly, achieving complete conversion in 0.6 min, and also results in the highest maximum reaction temperature of 139 °C and the highest

steady-state temperature of 76 °C. The Curie temperature of the cobalt particles (1130 °C) is much higher than the nickel particles (358 °C)[20] and therefore heats the resin faster and causes a more rapid reaction, resulting in the achievement of a higher maximum temperature. Nanoscale nickel particles heat the resin faster and reach a higher maximum reaction temperature as compared to micrometer-scale particles due to the increased susceptibility to the magnetic field. The different heating rates of the particles result in significantly different kinetic and temperature profiles, which demonstrate that induction curing is readily controlled by choosing different magnetic particles.

2. Temperature Profile Modeling. The polymerization reaction rate and final conversion of induction cured systems are strongly affected by temperature which is dictated by both the exothermic heat of reaction and the induction heating. Moreover, temperature gradients that are formed within the sample result in reaction rate gradients which reciprocally affect the temperature profile in the sample. Modeling of the temperature profile during induction curing helps to understand how factors, such as induction heater power, sample geometry, initiator, or resin formulation, affect the curing; predict the complex curing relationships; and enable better design of the formulations for specific application requirements, for example adhesion to temperature-sensitive substrates. Therefore, induction curing broadens the scope of radiation curing capabilities beyond that which is possible by conventional photoinitiated polymerizations.

The thiol−acrylate system is chosen for modeling because it maintains the advantages of thiol−ene systems while achieving higher glass transition temperatures, which facilitates applications in adhesives and coatings. TMPTMP−PEGDA with 1.5 wt % Ni (nm) is utilized as a model system with the polymer sandwiched between glass slides. The thickness of the polymer and glass is 0.76 and 0.1 mm, respectively, and this direction is defined as the x-direction. On the basis of the radical reaction mechanism, mass balances during curing are described as the consumption of initiator (eq 1), inhibitor (eq 2), monomer (eq 3), and radicals (eq 4).[21]

$$\frac{d[I]}{dt} = -k_d[I] \tag{1}$$

$$\frac{d[Z]}{dt} = -k_z[Z][P^\bullet] \tag{2}$$

$$\frac{d[M]}{dt} = -k_p[M][P^\bullet] \tag{3}$$

$$\frac{d[P^\bullet]}{dt} = R_i - 2k_t[P^\bullet]^2 - k_z[Z][P^\bullet] \tag{4}$$

in which [I], [Z], [M], and [P•] are the concentration of initiators, inhibitors, double bonds, and radicals, respectively; k_d, k_z, k_p, and k_t are the kinetic constants for initiation, inhibition, propagation, and termination, respectively. On the basis of the mixed reaction mechanism of the thiol−acrylate system, the consumption of the double bonds includes both acrylate homopolymerization and chain transfer to thiol. Several of the critical assumptions inherent in these mass balances are that (1) two primary radicals are generated by the initiation step, (2) chain length does not affect the propagation, termination, or inhibition steps, (3) bimolecular termination is the dominant mechanism for termination, and (4) the network is homogeneously formed and there is no significant diffusion that occurs during the reaction.[22]

Because of the induction heating process and the exothermic polymerization reaction, the temperature changes substantially during the curing. Each of the kinetic constants is written in an Arrhenius form (eq 5)[21]

$$k_i = k_{i0} \exp\left(\frac{-E_{ai}}{RT}\right) \tag{5}$$

where the subscript i refers to the initiation, inhibition, propagation, or termination reaction; k is the kinetic constant, k_0 is the pre-exponential factor, E_a is the activation energy, R is the gas constant, and T is the absolute temperature.

The energy balances are given in eqs 6 and 7. The assumptions inherent to the energy balance are that (1) conduction only occurs in the x-direction in the sample, (2) there is no significant convection or radiation, and (3) the decrease in heat generated by the particles with increased sample temperature is small enough that the heat generated by the particles can be considered to be constant throughout the reaction. The transient energy balances on the glass layers and the polymer layer are eqs 6 and 7, respectively.

$$\rho_{glass} C_{glass} \frac{\partial T}{\partial t} = k_{glass} \frac{\partial^2 T}{\partial x^2} \tag{6}$$

$$\rho_{poly/Ni} C_{poly/Ni} \frac{\partial T}{\partial t} = k_{poly/Ni} \frac{\partial^2 T}{\partial x^2} + Q_{IND} + Q_{REC} \tag{7}$$

Here, ρ is the density, C is the heat capacity, and k is the heat conductivity. The subscript describes different materials in the modeling: glass is glass surface and poly/Ni is the resin−nickel particle mixture. Q_{IND} and Q_{REC} are the heats generated by inductive heating of the particles and by the exothermic reaction, respectively. The boundary conditions are that the temperature at the glass surfaces contacting the polymer equals the temperature at the polymer surface and that the heat flux at the glass/polymer interface is equal to that at the glass/air interfaces (eq 8).

$$k_{glass} \frac{dT}{dx} = h_{air}(T - T_{air}) \tag{8}$$

Here, k_{glass} is the thermal conductivity of glass, h_{air} is the heat transfer coefficient, and T_{air} is the ambient temperature.

Q_{IND} is a function of the induction heater power, particle loading, and particle size and can be determined from the steady-state temperature of the cured sample. At steady state, the boundary condition at the glass surface contacting the polymer is that the total heat transfer from the polymer to the glass equals the heat generated by the particles (eq 9)

$$k_{glass} \frac{dT}{dx} A_{glass} = \frac{1}{2} Q_{IND} V_{polymer} \tag{9}$$

in which k_{glass} is the thermal conductivity of glass, A_{glass} is the area of the glass, Q_{IND} is the heat generated by induction heating, and $V_{polymer}$ is the polymer volume. The value of Q_{IND} is calculated from eqs 8 and 9, and Q_{IND} as a function of induction heater power is obtained by changing the power.

Figure 3a illustrates the heat generated by the particles versus induction heater power for both increasing and decreasing induction curing power. The results indicate that Q_{IND} exhibits

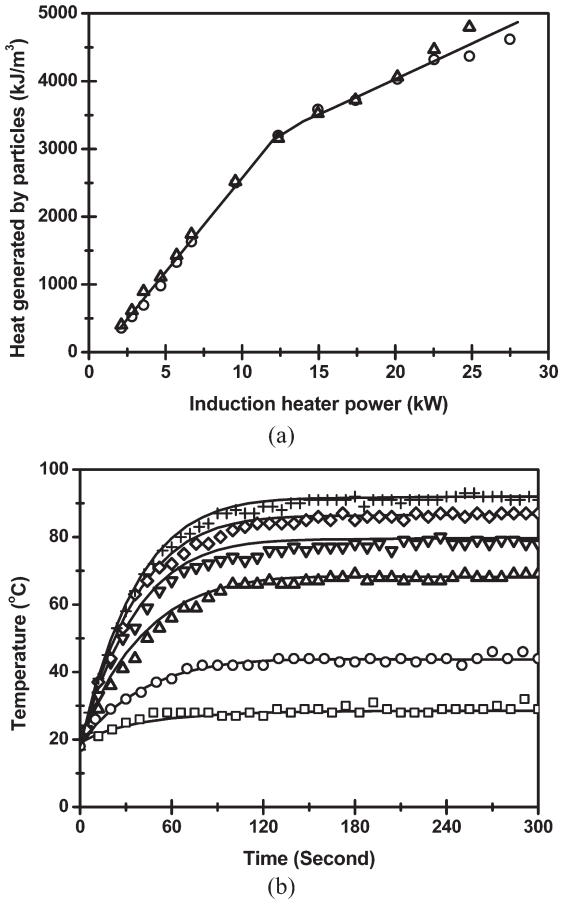

Figure 3. (a) Heat generated by particles in a fully cured polymer sample at different induction power levels during the process of increasing power (○) and during the process of decreasing power (Δ). The lines represent the data fit. (b) Experimental surface temperature profiles versus time for particles in cured polymer samples heated at (+) 28, (◇) 23, (▽) 17, (△) 12, (○) 7, and (□) 4 kW, along with the lines for the modeling predictions (—). The cured polymers are comprised of TMPTMP−PEGDA with 1.5 wt % Ni (nm) particles.

a linear relationship between induction heater power at steady state during the processes of increasing and decreasing power. There is no obvious difference between the data obtained from these two processes, which indicates that the thermal history does not have a significant effect on the heat generated by induction heating of the particles. Figure 3b shows the surface temperature profile versus time for the experimental and modeling results of the transient, nonreacting system.

The heat generated by the exothermic polymerization reaction is the product of the reaction enthalpy and the rate of double bond consumption (eq 10)

$$Q_{REC} = \Delta H \frac{d[M]}{dt} \quad (10)$$

in which ΔH is determined from the experimental results. The heat transfer profile for induction curing is obtained by simultaneously solving eqs 1−7 with the given boundary conditions and the parameters in Table 1 with the solution presented in Figure 4. The experimental and modeling results at different induction heater powers are extremely consistent with temperature differences of up to only 9 °C, with 7% average variation.

Table 1. Physical and Kinetic Parameters Used in Heat Transfer Modeling

parameter	value	unit	reference
k_{d0}	2.9×10^{15}	1/s	23
E_{ad}	130000	J/mol	23
k_{z0}	5.3×10^{7}	$m^3/(mol\ s)$	24
E_{az}	18000	J/mol	24
k_{t0}	3.6×10^{3}	$m^3/(mol\ s)$	24
E_{at}	2900	J/mol	24
k_{p0}	3000	$m^3/(mol\ s)$	experimentally determined[a]
E_{ap}	8900	J/mol	experimentally determined[a]
ρ_{glass}	2225	kg/m^3	25
C_{glass}	835	J/(kg K)	25
k_{glass}	1.4	W/(m K)	25
$\rho_{poly/Ni}$	1230	kg/m^3	calculated by volumetric ratio
$C_{poly/Ni}$	1541	J/(kg K)	calculated by volumetric ratio
$k_{poly/Ni}$	0.35	W/mK	calculated by volumetric ratio
h_{air}	25	$W/(m^2\ K)$	experimental fit
ΔH	36000	W/m^3	experimental fit

[a] Determined by photocuring of the same system at room temperature to maintain a constant temperature, since k_{p0} and E_{ap} are not related to the initiation mechanism.

After verifying the consistency of the modeling and experimental results, the model was utilized to predict reaction temperatures and polymerization kinetics for systems with varying thermal initiator concentration, initiator decay rate, monomer molecular weight, and temperature gradients in samples with varying thickness. Figure 5 shows the modeling results of surface temperature profile versus time for varying induction power. The data indicate that decreasing the power delays the onset of the polymerization reaction due to the slower rate of AIBN cleavage at lower temperatures. The reaction effectively begins after ∼60 s when the sample is heated with 20 kW as compared to the reaction initiating at ∼270 s when the sample is heated with 8 kW. A 20 °C difference in the maximum reaction temperatures is observed for polymerizations initiated by 20 and 8 kW power.

The initiation step is one of the tunable parameters that control the reaction kinetics and heat profile of induction curing. Here, the model is utilized to predict behavior for different initiator concentrations and initiators with different half-lives. Figure 6 shows the modeling results for the surface temperature profile as a function of time when the initiator concentration is varied. Decreasing the AIBN concentration delays the reaction onset because it takes longer to consume the inhibitor given the lower radical generation rate. The maximum reaction temperature is only minimally affected with lower AIBN concentrations leading to higher maximum temperatures due to the increased temperature at which the polymerization reaction escalates. Figure 7a shows the modeling results for the surface temperature profile versus time when using different thermal initiators with varying activation energies and decay rates. The half-life and kinetic constants utilized in modeling these initiators are listed in Table 2. The onset of the polymerization reaction is delayed by reducing the initiator decomposition rate. Di(2-ethylhexyl) peroxydicarbonate (DTBP) exhibits the shortest half-life (2 min at 90 °C) among these four initiators and as a result initiates the reaction at a lower temperature than all of the other initiators and exhibits a lower maximum temperature resultant from the

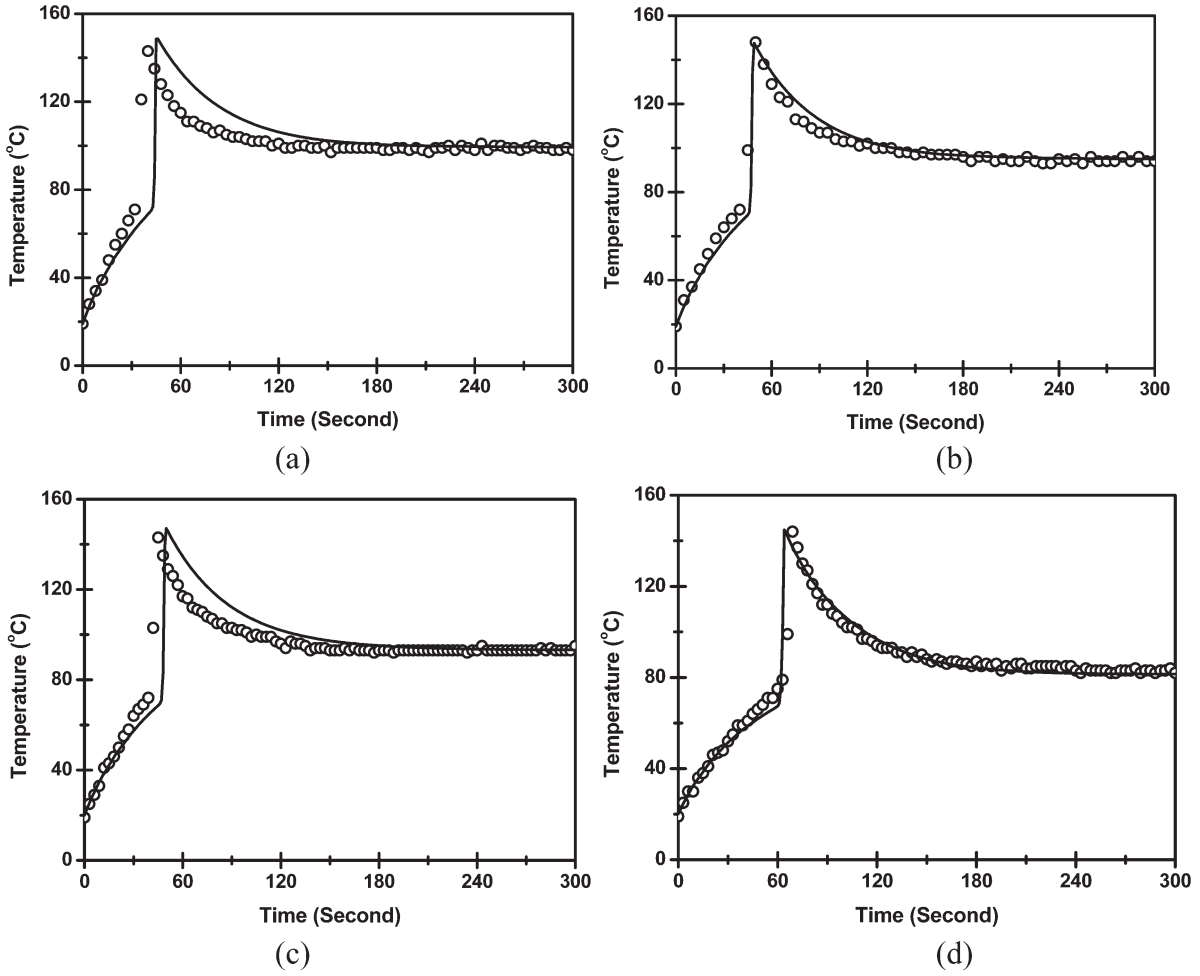

Figure 4. Surface temperature profile versus time for (○) experimental data and (—) modeling results of TMPTMP−PEGDA with 1 wt % AIBN and 1.5 wt % Ni (nm) cured with varying induction heater powers: (a) 32, (b) 30, (c) 27, and (d) 20 kW.

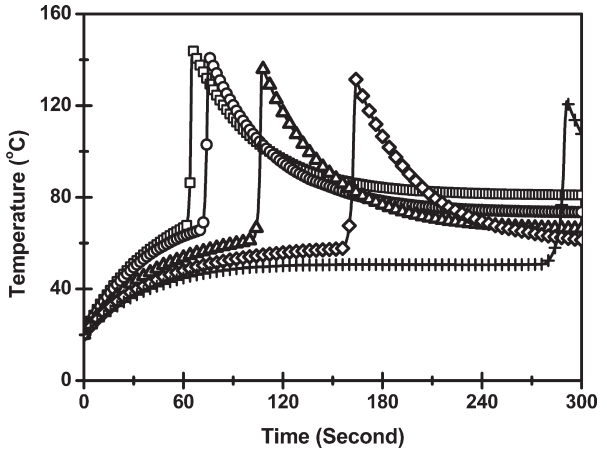

Figure 5. Modeling results of surface temperature profile versus time of TMPTMP−PEGDA with 1 wt % AIBN and 1.5 wt % Ni (nm) cured by varying induction power: (□) 20, (○) 15, (△) 12, (◇) 10, and (+) 8 kW.

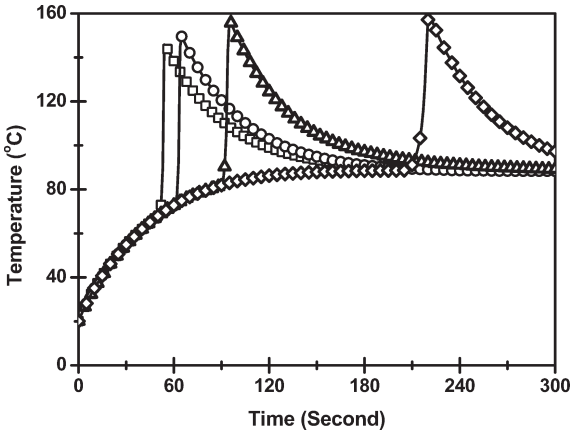

Figure 6. Modeling results of surface temperature profile versus time for TMPTMP−PEGDA with 1.5 wt % Ni (nm) initiated by 25 kW and (□) 1, (○) 0.5, (△) 0.1, and (◇) 0.01 wt % AIBN.

reaction onset occurring at the lower temperature. The maximum temperatures of polymerizations initiated by AIBN (half-life of 20 min at 90 °C) and 1,1′-azodi(hexahydrobenzonitrile) (AHBN) (half-life of 4.8 h at 90 °C) increase because the polymerization onset is delayed to higher temperatures. Di-(*tert*-butylperoxyisopropyl)benzene (BPIPB) has the longest half-life (10 days at 90 °C) among these four initiators but exhibits a much lower maximum temperature. This outcome is because the reaction time scale (20 min) is very short compared

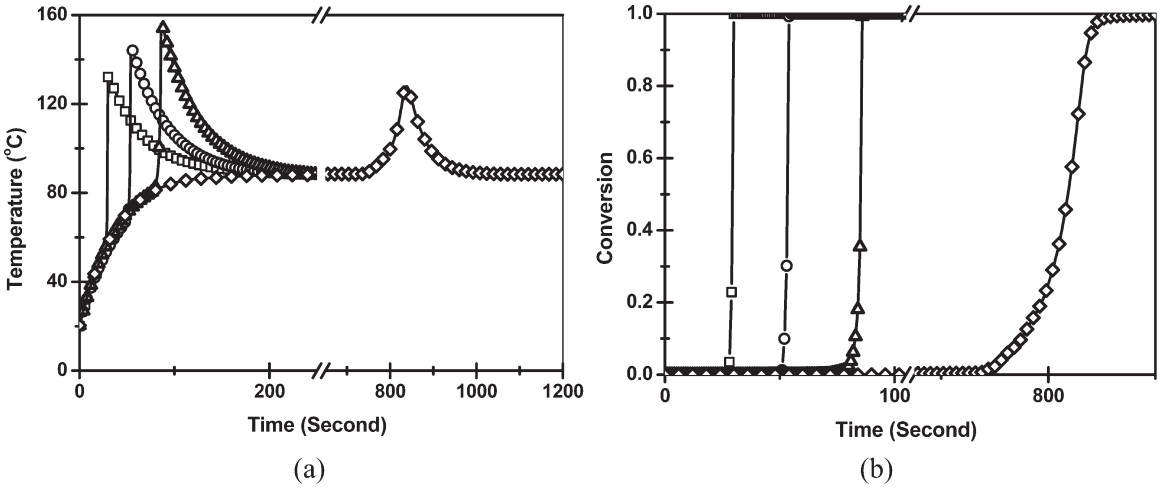

Figure 7. Modeling results of (a) surface temperature profile versus time and (b) conversion versus time of TMPTMP−PEGDA with 1 wt % initiator and 1.5 wt % Ni (nm) at 25 kW with (□) DTBP, (○) AIBN, (△) AHBN, and (◇) BPIPB.

Table 2. Activation Energy, Prefactor of Kinetic Constant, and Half-Life of Initiators[23]

initiator	E_a (J/mol)	k_{d0} (1/s)	half-life at 90 °C
di(2-ethylhexyl) peroxydicarbonate (DTBP)	126 000	7.4×10^{15}	2 min
2,2′-azobis(isobutyronitrile) (AIBN)	130 000	2.9×10^{15}	20 min
1,1′-azodi(hexahydrobenzonitrile) (AHBN)	142 000	1.1×10^{16}	4.8 h
di(*tert*-butylperoxyisopropyl)benzene (BPIPB)	153 000	7.7×10^{15}	10 days

with the 10 day half-life of AHBN at 90 °C. Thus, a steady state temperature from particle heating is reached due to the slow reaction rate. Figure 7b illustrates the slow reaction rates of systems initiated by BPIPB. BPIPB systems require 3 min to achieve full conversion of double bonds while the other three systems require less than 10 s to achieve full conversion once the polymerization reaction is initiated.

In addition to the initiation step, the monomer formulation also affects the temperature profile and reaction kinetics of induction curing. Figure 8 shows the modeling results for the surface temperature profile versus time for samples with different molecular weight PEGDA monomers. The maximum temperature decreases with increasing molecular weight of PEGDA, resulting from the decreased double-bond concentration leading to a slower reaction rate and less heat generated by the reaction. On the basis of these modeling results, the polymerization kinetics and the maximum reaction temperature are readily controlled by the induction heater power, the thermal decomposition kinetics of the initiator, and the molecular weight and functionality of the monomers.

Sample thickness is another important factor that affects the temperature and reaction kinetics. When a thick sample is thermally cured, a significant temperature gradient arises in the sample due to heat transfer, which results in a corresponding gradient in the polymerization rate. Since the heat generated by the reaction is proportional to the reaction rate, the reaction rate gradient reciprocally affects the temperature profile in the

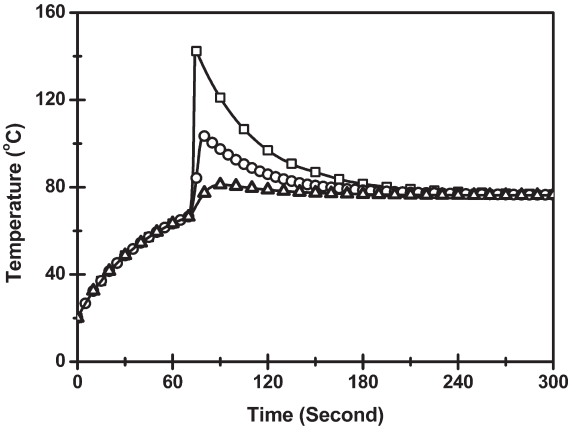

Figure 8. Modeling results for the surface temperature profile versus time of TMPTMP−PEGDA with 1 wt % AIBN and 1.5 wt % Ni (nm) cured at 17 kW with PEGDA molecular weights of (□) 302, (○) 700, and (△) 2000 g/mol.

sample. As temperature and conversion gradients can have a dramatic impact on material properties, it is of interest to study the temperature profiles of thick samples cured by induction heating. Figure 9 shows bulk temperature profiles at a cross section of the samples during curing. Because of the uniform nature of the energy generation associated with the induction curing mechanism, there is only a 4 °C temperature gradient in a 0.76 mm thick sample (Figure 9a) at the fastest reaction rate and a 17 °C temperature gradient in an even larger, 1.2 mm thick sample (Figure 9b).

3. Carbon Nanotube Composite Systems. Induction heating was utilized to cure thiol−acrylate−carbon nanotube composite systems. Composite systems with carbon nanotubes cannot be cured by photopolymerization due to the strong light attenuation associated with light absorption by the carbon nanotubes. To obtain appropriate dispersion, hydroxyl functionalized carbon nanotubes were added to the TMPTMP−PEGDA monomer resin because the hydroxyl group hydrogen bonds with the ether group in PEGDA to promote enhanced dispersion. SEM results of the cured polymer (Figure 10) demonstrate

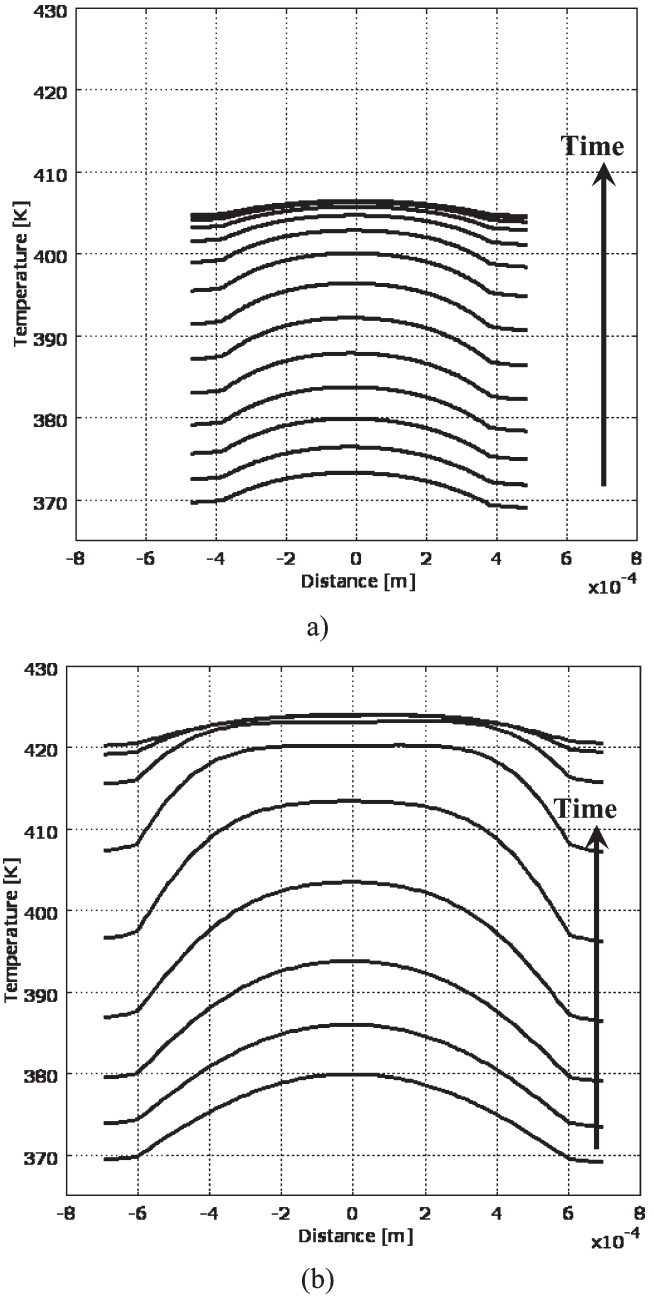

Figure 9. Modeling results of bulk temperature profile versus distance at a cross section of TMPTMP−PEGDA initiated by 1 wt % AIBN and 1.5 wt % Ni (nm) particles at 17 kW with temperature data presented for 0.1 s intervals during the exothermic reaction phase: (a) 0.76 mm thickness sample presented from 162.4 to 163.7 s and (b) 1.2 mm thickness sample from 86.5 to 87.3 s.

dispersion of the carbon nanotubes and the nanoscale nickel particles in the TMPTMP−PEGDA sample. Here, the composite containing 0.1 wt % carbon nanotubes in TMPTMP−PEGDA reaches 92% conversion. When the amount of CNTs is increased to 1 wt %, the sample is totally absorptive, and the IR signal cannot penetrate through the sample to determine the conversion. However, the maximum reaction temperature of the sample containing 1 wt % carbon nanotubes TMPTMP−PEGDA is similar to the sample containing 0.1 wt % carbon nanotubes, indicating that a similar conversion was likely achieved. Figure 11 shows that the

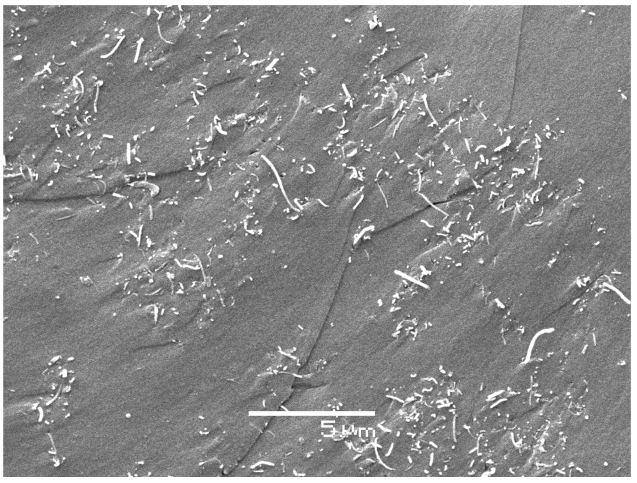

Figure 10. SEM image of TMPTMP−PEGDA with 1 wt % AIBN, 1 wt % Ni (nm), and 1 wt % CNT-OH scanned at low vacuum mode 5 kV.

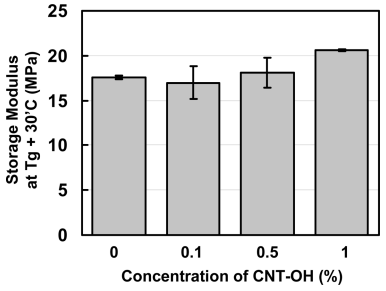

Figure 11. Storage modulus at T_g + 30 °C for varying amounts of CNT-OH in TMPTMP−PEGDA with 1 wt % AIBN and 1 wt % Ni (nm). The sample is cured at 22 kW.

rubbery storage modulus slightly increases to 21.6 ± 0.1 MPa with 1 wt % carbon nanotubes as compared to 17.6 ± 0.2 MPa for the sample without carbon nanotubes. The electrical conductivity increases by at least 6 orders of magnitude with 1 wt % carbon nanotubes (0.33 ± 0.05 S/m) as compared to $<10^{-7}$ S/m for the pure TMPTMP−PEGDA.

CONCLUSIONS

In this work, we have demonstrated a new type of radiation curing based on induction heating of thiol−ene and thiol−acrylate systems with ferromagnetic particles. A model was developed that accurately predicts both temperature profiles and polymerization rates of samples with varying particle types and sizes, induction heater power, initiator type and concentration, functional group concentration, and sample geometry. Thiol−ene and thiol−acrylate composite systems containing carbon nanotubes, which are completely opaque and uncurable by photocuring, were demonstrated to be readily polymerized by induction heating. The addition of only 1 wt % carbon nanotubes increased the storage modulus and resulted in an electrically conductive composite.

AUTHOR INFORMATION

Corresponding Author

*Ph 303-492-3247, Fax 303-492-4341, e-mail christopher.bowman@colorado.edu.

■ ACKNOWLEDGMENT

The authors gratefully acknowledge the National Science Foundation CBET 0626023 and National Institutes of Health/ National Institute of Dental and Craniofacial Research Grant DE10959 for funding this work.

■ REFERENCES

(1) Hoyle, C. E.; Lee, T. Y.; Roper, T. *J. Polym. Sci., Part A: Polym. Chem.* **2004**, *42*, 5301.
(2) Kloosterboer, J. G. *Adv. Polym. Sci.* **1988**, *84*, 1.
(3) Fouassler, J. P. *Radiation Curing in Polymer Science and Technology I, Fundamentals and Method*; Elsevier Applied Science: London, 1993; Chapter 1.
(4) Rapoport, E.; Pleshivtseva, Y. *Optimal Control of Induction Heating Processes*; Taylor & Francis: Boca Raton, FL, 2007; Chapter 1.
(5) Willard, M. A.; Francavilla, T.; Harris, V. G. *J. Appl. Phys.* **2005**, *97*, 10F502.
(6) Karapetoff, V. *Example of Core Loss of Iron*, 2nd ed.; John Wiley & Sons: New York, 1993; Chapter 13.
(7) Suwanwatana, W.; Yarlagadda, S.; Gillespie, J. W. *Compos. Sci. Technol.* **2006**, *66*, 2825.
(8) Lozinskii, M. G. *Industrial Applications of Induction Heating*; Pregamon Press: London, 1969; Chapter 1.
(9) Zinn, S.; Semiatin, S. L. *Elements of Induction Heating: Design, Control, and Applications*; Electric Power Research Institute: Palo Alto, CA, 1988; Chapter 1.
(10) Martinazzo, F.; Montebelluna. US20050123743A1, 2005
(11) Schmidt, A. M. *Macromol. Rapid Commun.* **2006**, *27*, 1168.
(12) Yakacki, C. M.; Satarkar, N. S.; Gall, K.; Likos, R.; Hilt, J. Z. *J. Appl. Polym. Sci.* **2009**, *112*, 3166.
(13) Tay, T. E.; Fink, B. K.; McKnight, S. H.; Yarlagadda, S.; Gillespie, J. W. *J. Compos. Mater.* **1999**, *33*, 1643.
(14) Suwanwatana, W.; Yarlagadda, S.; Gillespie, J. W. *Compos. Sci. Technol.* **2006**, *66*, 1713.
(15) Bowman, C. N.; Kloxin, C. J. *AIChE J.* **2008**, *54*, 2775.
(16) Hoyle, C. E.; Bowman, C. N. *Angew. Chem., Int. Ed.* **2010**, *49*, 1540.
(17) Hoyle, E. C.; Lowe, A. B.; Bowman, C. N. *Chem. Soc. Rev.* **2010**, *39*, 1355.
(18) Cramer, N. B.; Bowman, C. N. *J. Polym. Sci., Part A: Polym. Chem.* **2001**, *39*, 3311.
(19) Moniruzzaman, M.; Winey, K. I. *Macromolecules* **2006**, *39*, 5194.
(20) Bozorth, R. M. *Ferromagnetism*; IEEE Press: New York, 1978; Chapter 8.
(21) Odian, G. *Principles of Polymerization*, 4th ed.; John Wiley & Sons: Hoboken, NJ, 2004; Chapter 3.
(22) Cramer, N. B.; Davies, T.; O'Brien, A. K.; Bowman, C. N. *Macromolecules* **2003**, *36*, 4631.
(23) Initiator manuals of Akzo Nobel Corporation.
(24) Goodner, M. D.; Bowman, C. N. *Chem. Eng. Sci.* **2002**, *57*, 887.
(25) Incropera, F. P.; Dewitt, D. P.; Bergman, T. L.; Lavine, A. S. *Introduction to Heat Transfer*, 5th ed.; John Wiley & Sons: Hoboken, NJ, 2007; p 745.